IEEE Access
Multidisciplinary : Rapid Review : Open Access Journal

Received October 30, 2018, accepted November 21, 2018, date of publication November 28, 2018,
date of current version December 27, 2018.

Digital Object Identifier 10.1109/ACCESS.2018.2883590

Wideband Full-Corporate-Feed Waveguide Continuous Transverse Stub Antenna Array

QINGCHUN YOU[1], (Student Member, IEEE), YUNLONG LU[1,2], YANG YOU[1], YI WANG[3], (Senior Member, IEEE), ZHANG-CHENG HAO[2], (Senior Member, IEEE), AND JIFU HUANG[1]

[1]Faculty of Electrical Engineering and Computer Science, Ningbo University, Ningbo 315211, China
[2]State Key Laboratory of Millimeter Waves, Southeast University, Nanjing 210096, China
[3]School of Engineering, University of Birmingham, Birmingham B15 2TT, U.K.

Corresponding author: Yunlong Lu (luyunlong@nbu.edu.cn)

This work was supported in part by the National Natural Science Foundation of China under Projects 61631012 and 61801252, in part by the Natural Science Foundation of Zhejiang Province under Project LQ17F010002, and in part by the K.C. Wong Magna Fund in Ningbo University. The work of Y. Wang and Z.-C. Hao was supported by the National Natural Science Foundation of China under Grant 61628104.

ABSTRACT A Ka-band waveguide continuous transverse stub antenna array with full-corporate-feed network is presented in this paper. Multiple-section stepped-impedance transformers are used for wideband impedance matching of the radiation slots. The required high-quality quasi-TEM wave excitation is generated by a wideband plane-wave generator (WPWG). Compared with the conventional pillbox structure, the WPWG produces a quasi-TEM wave with more uniform amplitude distribution. By using the combination of these design features, significant increases both in bandwidth and antenna aperture efficiency are achieved. For demonstration, a prototype is designed, fabricated, and measured. Excellent agreement is achieved between simulations and measurements. The antenna is matched over the entire Ka-band of 26–40 GHz. A high antenna aperture efficiency of over 75% and a low cross-polarization of less than −46 dB are achieved over the entire bandwidth. The demonstrated features of wideband, high aperture efficiency, and low cross-polarization have great potentials for millimeter-wave applications.

INDEX TERMS Wideband antenna array, continuous transverse stub antenna, aperture efficiency, wideband plane wave generator, full-corporate-feed network.

I. INTRODUCTION

The millimeter-wave (MMW) frequencies of 26.5-29.5 GHz and 37-40 GHz, contained in Ka-band, have been allocated to new 5G radio access [1]. The Ka-band itself has already been widely used in satellite communications. Wideband high gain antennas with low cross-polarization and high aperture efficiency are highly desired for such applications [2], [3]. Microstrip, substrate-integrated waveguide (SIW) and hollow waveguide antennas are the common technologies. At these high frequencies, the microstrip lines and SIW waveguides experience high dielectric losses in the feeding network. The losses become critically significant when designing large feeding networks for high-gain antenna arrays [4]–[7]. Hollow waveguide has much lower losses in general and slotted waveguide (SW) array has been a good choice for high performance MMW antennas. But SW arrays commonly suffer from a narrow bandwidth [8]–[12]. Recently, a diffusion bonding based fabrication technology has been applied to SW arrays, and the achieved bandwidth varied between 10% and 19% [13]–[15]. Ridge gap waveguide technology has also been used in wideband MMW antenna array design [16]. A gain of over 27.5 dBi was achieved over a 30% impedance bandwidth (50–67.8 GHz).

Continuous transverse stub (CTS) antenna arrays have long been considered a competitive hollow-waveguide technology for high gain and high efficiency antennas at MMW frequencies [17], [18]. Some work has been done in the past few years. A 32-slot CTS antenna array with 19% impedance bandwidth from 71-86 GHz was shown in [19]. In [20], a CTS antenna array based on low temperature co-fired ceramic (LTCC) technology was reported. The antenna realized over 25% fractional bandwidth from 51.2-66 GHz. Most of these CTS antennas adopted a pillbox coupler configuration as the TE_{10} to quasi-TEM wave converter. Due to the relatively

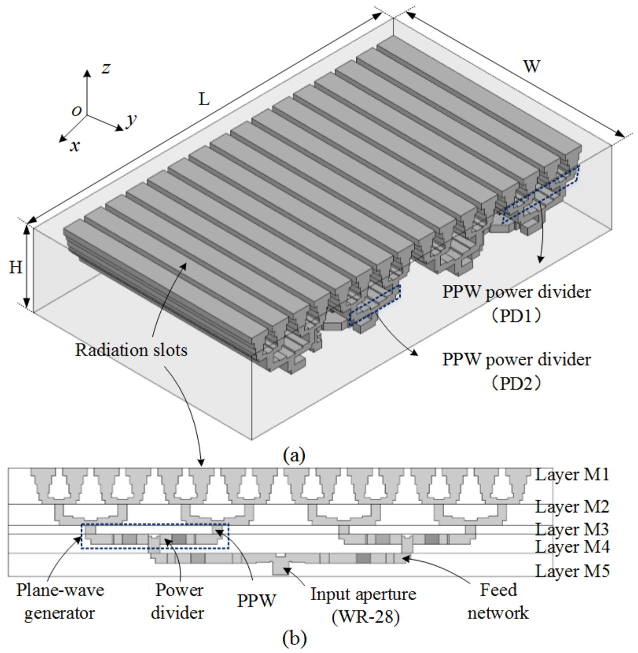

FIGURE 1. Configuration of the proposed CTS array. (a) 3-D overview; (b) Cross-sectional view. It should be noted that the grey areas are the 'air cavities'.

narrow band characteristic of such a converter, the reported bandwidth of CTS and SW antennas so far was limited to 30 %. In addition, the amplitude distribution of the pillbox coupler normally exhibits a fall-off at the aperture edges, which causes significant reduction in the antenna aperture efficiency.

In this paper, a CTS antenna array with over 42% fractional bandwidth from 26-40 GHz covering the whole Ka-band is presented. Unlike the conventional pillbox coupler, a multiple-port excited wideband plane-wave generator (WPWG) is proposed to boost the conversion bandwidth from TE_{10} to high quality quasi-TEM wave. The amplitude distribution of the WPWG is examined in detail. By combining the wideband radiation structures with a full-corporate-feed networks, the bandwidth of the whole CTS antenna array has been significantly enhanced. In addition, with a more uniform amplitude distribution of the WPWG, the antenna aperture efficiency has been shown to improve effectively. To validate the design, a prototype array operating at Ka-band is fabricated and measured.

II. ANTENNA DESIGN AND ANALYSIS

The configuration of the proposed wideband CTS antenna array is shown in Fig. 1. It contains sixteen radiation slots and a full-corporate-feed network. The signal flow in the antennas is as follows:

1) The signal coming from the standard WR28 input waveguide port is divided into multiple paths by a 1-to-8 feed network in M5. A good impedance matching is required between the input hollow-waveguide and single-ridge waveguide.
2) The feed network is followed by two wideband plane-wave generators (WPWGs) in M3 and M4. The WPWG converts the TE_{10} mode in the single-ridge waveguide into a quasi-TEM wave in PPW with a wide operating band and uniform amplitude distribution. It is noted that the width of the CTS array is determined by the total width of the PPW in the WPWG, and it can be extended by adding the number of the excitation ports.
3) The four quasi-TEM wave outputs from M3 enter into four PPW power dividers in M2. Each of the divider outputs feeds into two radiation slots. The number of PPW power dividers is determined by the number of radiation slots.
4) Finally, the electromagnetic wave radiates from the sixteen CTS slots in M1. A multiple-section stepped impedance transformer (MSSIT) is loaded at each radiation slot to increase the operating bandwidth. The length of the radiation slots determines the number of the divisions in the feeding network. 8 divisions are needed in M5 in this design.

Next the radiation slot, PPW power divider, WPWG and feed network will be discussed in more details.

A. RADIATION SLOTS AND PPW POWER DIVIDERS

The radiation performance of the array is mainly determined by the radiation slot width a and period d_x shown in Fig. 2. According the analysis in [21], for broadband operation, the value of d_x/a should be close to 1. This means that the metal wall between the adjacent radiation slots should be as thin as possible. In consideration of the manufacturability, the value of d_x/a is set to be 1.4 in this design. To avoid grating lobes over the whole operating band, the period d_x should be less than the free-space wavelength of the highest operating frequency. In this work, the array is designed to operate over the entire Ka-band (26 to 40 GHz). With the free-space wavelength of 7.5 mm at 40 GHz, we choose $d_x = 7$ mm and $a = 5.5$ mm.

Fig. 2(a) shows the radiation unit, consisting of two radiation slots, two multiple-section stepped impedance transformer (MSSITs) and a PPW power divider in layer M1. The MSSIT is used to realize a wideband impedance matching between the radiation slot and output of the PPW power divider (named PD1). Fig. 3 shows the equivalent circuit of the MSSIT. The reflection coefficient from the input of the MSSIT can be calculated as [22]:

$$|\Gamma(\theta)| = \begin{cases} |\Gamma_0 \cos N\theta + \cdots + \\ \Gamma_n \cos(N-2n)\theta + \cdots + \frac{1}{2}\Gamma_{N/2}|, & N \in even \\ |\Gamma_0 \cos N\theta + \cdots + \Gamma_n \cos(N-2n)\theta \\ + \cdots + \Gamma_{(N-1)/2} \cos\theta|, & N \in odd \end{cases} \tag{1}$$

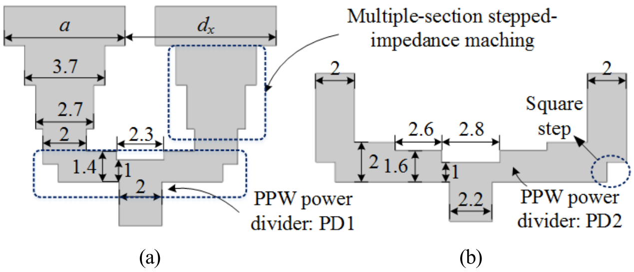

FIGURE 2. (a) Radiation unit; (b) PPW power divider in M2. All dimensions are given in millimeters.

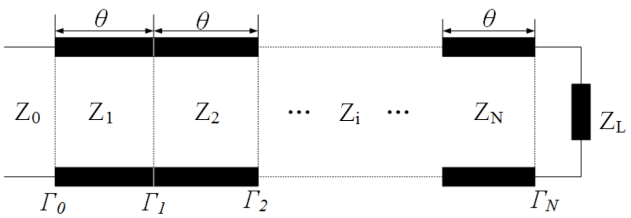

FIGURE 3. Equivalent circuit of the MSSIT.

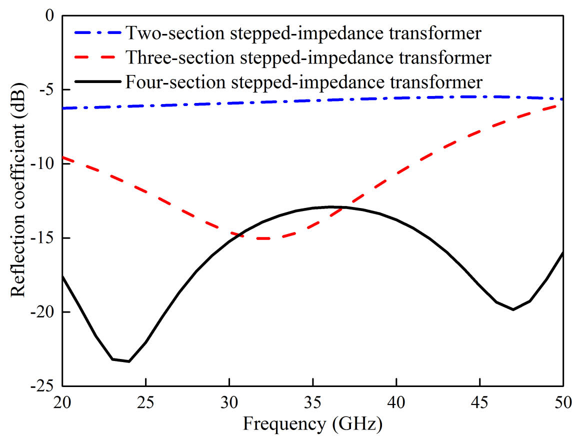

FIGURE 4. Impedance matching under different number of MSSIT.

where $\Gamma_i = (Z_{i+1}-Z_i)/(Z_{i+1}+Z_i)$, $i = 0, 1, 2, \ldots N$ is the total section number. Z_i is the characteristic impedance of the i-th line section, and Z_L ($120\pi\,\Omega$ in free-space) is the load.

Fig. 4 shows the simulated reflection coefficient of the MSSIT with different numbers of sections. It can be seen that the bandwidth increases with the number of sections. When this number is more than 3, the impedance bandwidth ($|S_{11}| < -10$ dB) can cover the whole Ka-band.

There are two types of PPW power dividers, namely PD1 and PD2, in layer M1 and M2, as shown in Fig. 2 (a) and (b) respectively. PD1 and PD2 form a four-way divider and feed the MSSITs to excite the radiation slots. It is noted that the width of the input port of PD2 is the same as the height of the PPW in the WPWG (shown in Fig. 9), which is also equal to the height of the single-ridge waveguide. In this way, no extra transition structure is needed between the input of PD2 and the output of WPWG (shown in Fig. 1). As the operating band of the single-ridge waveguide covers the Ka-band, its cutoff frequency is lower than 26 GHz. Thus, the height of the single-ridge waveguide is chosen to be 2.2 mm. Besides, a square step (shown in Fig. 2) is added at the bend of the output PPW to improve the impedance matching [23]. The optimized dimensions of the radiation units and PD2 are given in Fig. 2. The simulated reflection coefficients of PD1, PD2 and the radiation unit are shown in Fig. 5. The reflection coefficient of the radiation unit is lower than −22 dB.

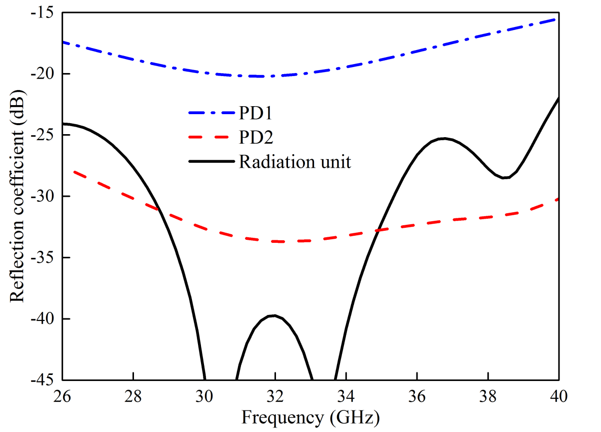

FIGURE 5. Simulated reflection coefficients of the radiation unit and the PPW power divider in M1, M2.

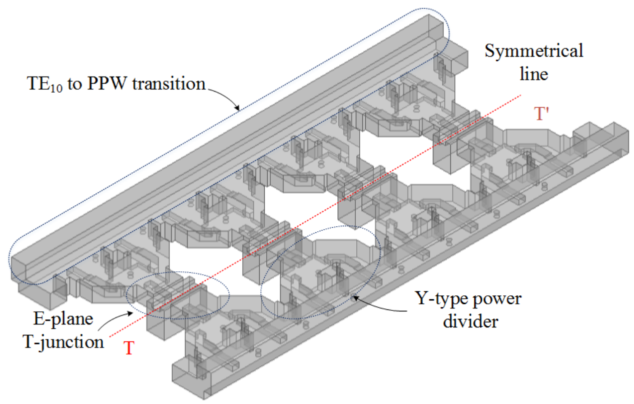

FIGURE 6. Structure of the wideband plane wave generator (WPWG).

B. WIDEBAND PLANE WAVE GENERATOR

The WPWG is employed to generate quasi-TEM wave as required to excite the radiation slots. Fig. 6 is the 3D-view of the proposed structure. It consists of four 1-to-4 single-ridge waveguide power dividers and two PPWs excited by 8 ports. It is worth mentioning that one WPWG generates two ways of quasi-TEM wave, because the symmetrical distribution of output ports in the 1-to-4 power dividers. The bandwidth of the WPWG should cover 26-40 GHz. Next, we will discuss

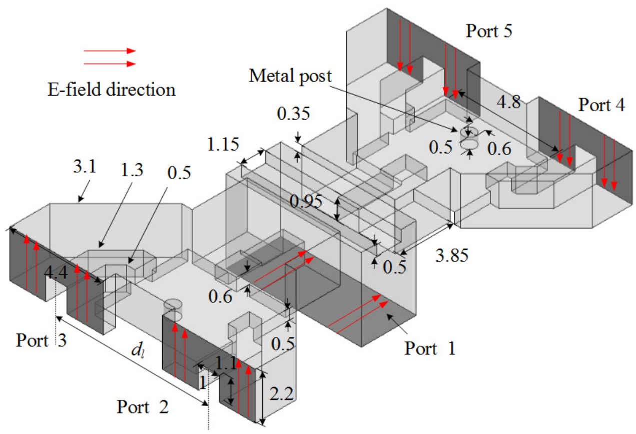

FIGURE 7. 1-to-4 single-ridge waveguide power divider. All dimensions are given in millimeters.

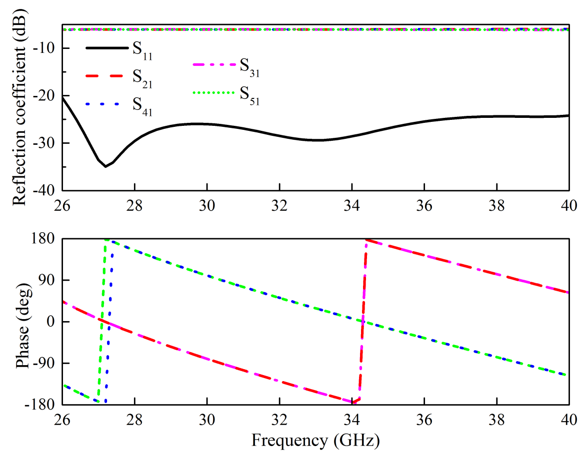

FIGURE 8. Simulated results of the 1-to-4 single-ridge power divider.

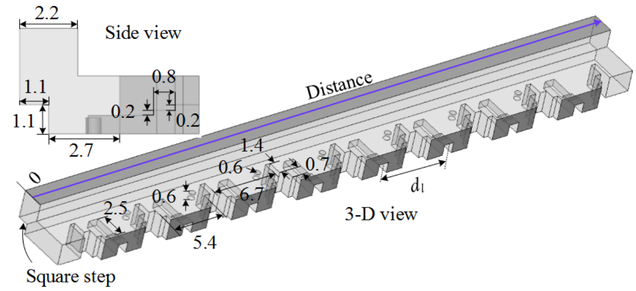

FIGURE 9. The PPW with eight excitation ports. All dimensions are given in millimeters.

the 1-to-4 single-ridge power divider and the TE_{10} to quasi-TEM wave converter in more details.

1) 1-TO-4 SINGLE-RIDGE WAVEGUIDE POWER DIVIDER

To achieve a good radiation performance, the generated quasi-TEM waves in the adjacent PPWs should have equal amplitudes and phases. As shown in Fig. 7, the 1-to-4 single-ridge waveguide power divider consists of one E-plane T-junction and two Y-type power dividers. The outputs from the E-plane T-junction are out of phase. This translates to the out-of-phase outputs between port 2(3) and 4(5). These outputs feed into the PPWs via right-angle bends, which bring the E-fields in the PPW back in alignment. By adjusting the distance (d_l) between the output ports, the amplitude distributions of the quasi-TEM waves in the PPWs can be optimized (more details given later). An inductive metallic post is loaded to the Y-type power divider to enhance the isolation between the output ports.

With the optimized dimensions given in Fig. 7 (d_l is set to be 7.2 mm), the simulated results of the 1-to-4 single-ridge power divider are given in Fig. 8. The reflection coefficient is lower than −20 dB and all the transmission coefficients are within -6 ± 0.05 dB over the entire Ka band. The output signals are in-phase between ports 2 (4) and 3 (5), but out-of-phase between ports 2 (3) and 4 (5).

2) TE_{10} TO QUASI-TEM WAVE CONVERTER

The electromagnetic wave with TE_{10} mode from the output ports of the 1-to-4 single-ridge power dividers are combined and converted to quasi-TEM wave in the PPWs. This is achieved by using 8 excitation ports, shown in Fig. 9. The signals at the 8 excitation ports are in-phase, which are guaranteed by the structure of WPWG and feed networks (shown in section II-C). To improve the amplitude balance of the quasi-TEM wave, a row of inductive metallic posts are loaded between the ridges to reduce the mutual interferences between adjacent ports. Besides, a square step is also added to the bend of the PPW.

The amplitude distribution of the quasi-TEM wave along the PPW has been optimized to achieve a minimum imbalance over the whole Ka band. This is mainly done by adjusting d_l, and similar treatment was detailed in our previous work [24]. In this design, d_l is chosen to be $0.8\lambda_0$ (7.2 mm). As a result, the width of the PPW becomes 63 mm. Two $\lambda_0/4$ (λ_0 is the free space wavelength at the center operating frequency) terminating offsets are added at both ends of the PPW to reduce the reflections and further improve the amplitude distribution [25]. Fig. 10 shows the E-field amplitude imbalance with or without the terminating offsets at the center frequency of 33 GHz. With the offset, the amplitude fluctuation can be effectively reduced. Fig. 11 shows the E-field distribution at different frequencies along the y-axis in the PPW (as indicated in Fig. 9). It is evident that the amplitude fluctuation is kept under 1.5 dB across the whole Ka-band.

C. FEED NETWORK

A 1-to-8 power divider is designed in M5 to feed the WPWG. Fig. 12 shows the configuration of the feed network. An E-plane T-junction at the center is cascaded with two-stage single-ridge waveguide H-plane T-junctions. At each output port, three is a transition structure between single-ridge waveguide and hollow waveguide. Note that the phases between the outputs of the E-plane T-junction are also

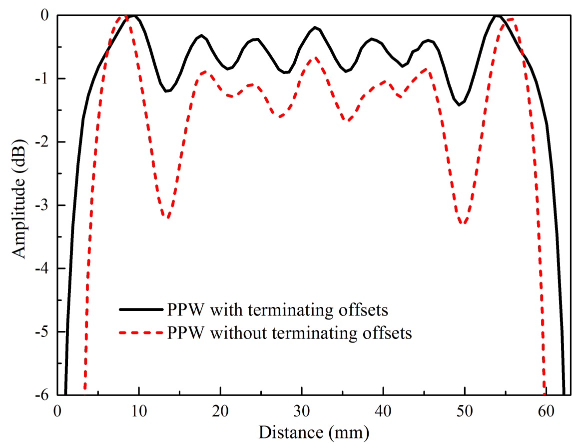

FIGURE 10. E-field amplitude fluctuation with and without the $\lambda_0/4$ terminating offsets at 33 GHz.

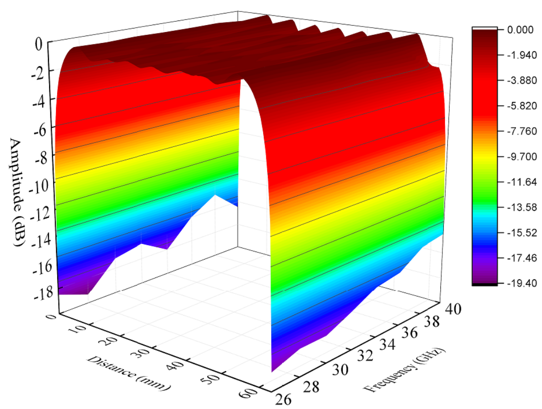

FIGURE 11. E-field variation of the quasi-TEM wave in the PPW over the frequency band of 26-40 GHz.

opposite. But with the symmetrical distribution of the eight output ports, the phase differences between the ports 2, 3, 4, 5 and ports 6, 7, 8, 9 are reversed to be in-phase. The E- and H-plane T-junctions, as well as the transition structure are also shown separately in Fig. 12. To maintain wideband impedance matching, a capacitive board, marked out in Fig. 12(c), is embedded in each of the H-plane T-junction and two three-section impedance transformers are used [24], [25].

In order to realize wideband transition between the single-ridge waveguide and the hollow waveguide, a stepped ridge and hollow waveguide are involved. A square step is again loaded to the bend for matching [23]. The matching is mainly controlled by the heights of the stepped ridge and hollow waveguide: C_h and R_h, as shown in Fig. 13. The parameters study of this transition structure can be found in Fig. 13. When $C_h = 1.16$ mm and $R_h = 0.8$ mm, a reflection coefficient lower than -24 dB can be achieved over the bandwidth of 26 - 40 GHz.

The simulated amplitude responses of the 1-to-8 power divider are given in Fig. 14. The reflection coefficient is lower than -16 dB and all the transmission coefficients are

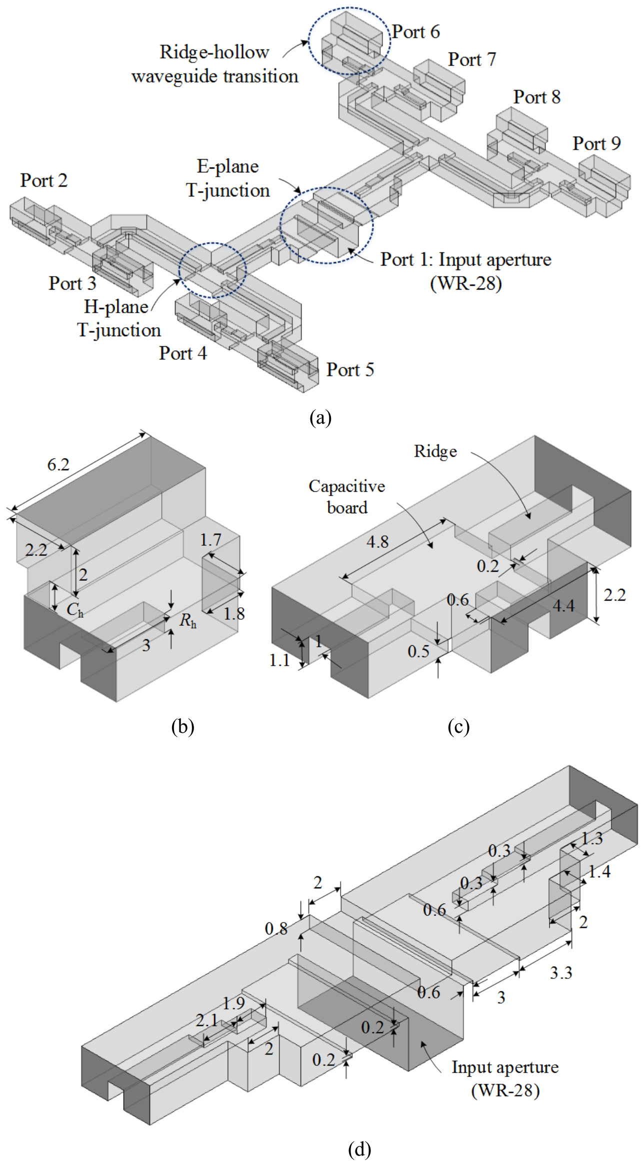

FIGURE 12. (a) 1-to-8 feed network; (b) Transition of single-ridge waveguide to hollow waveguide; (c) H-plane T-junction; (d) E-plane T-junction. All dimensions are given in millimeters.

within -9 ± 0.05 dB, exhibiting a good matching and output amplitude balance over the bandwidth of 26 to 40 GHz.

III. MEASUREMENTS AND DISCUSSION

The CTS antenna has been prototyped using aluminum blocks. To simplify the assembly, the layers M1 and M2 are merged to one block. A set of tightening screws are placed around the antenna to suppress wave leakage. The photographs of layers M1-M5 and the assembled CTS antenna array are given in Fig. 15. The overall sizes of the fabricated CTS antenna array are 126.5 mm × 79 mm × 30 mm (L×W×H, shown in Fig. 1(a)). All the simulations are carried out with Ansoft HFSS. The radiation performances are measured using a small near-field vertical planar scanner system from NSI-MI Technologies.

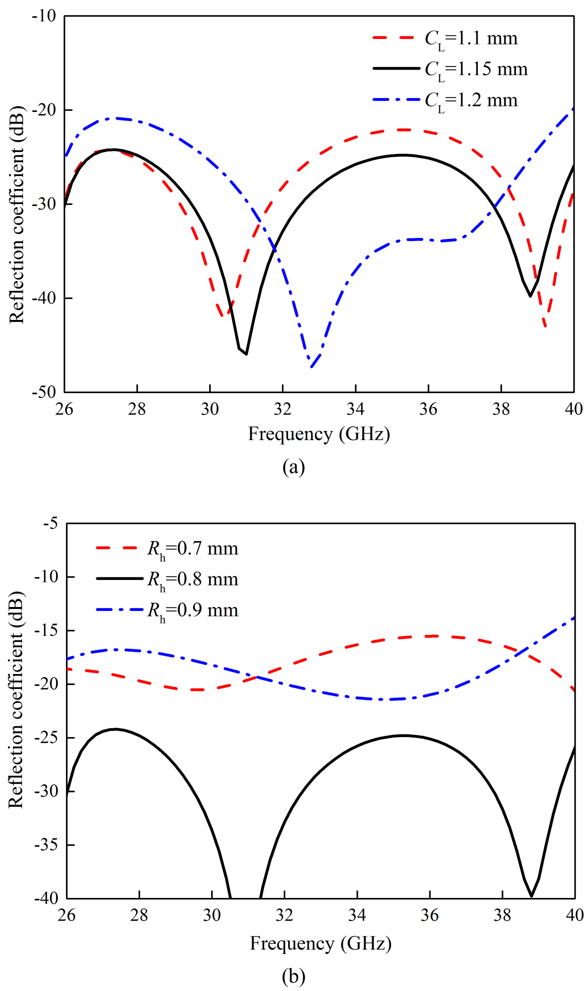

FIGURE 13. Impedance matching analysis of the transition structure in Fig. 12 (b): (a) different values of C_h, (b) different values of R_h.

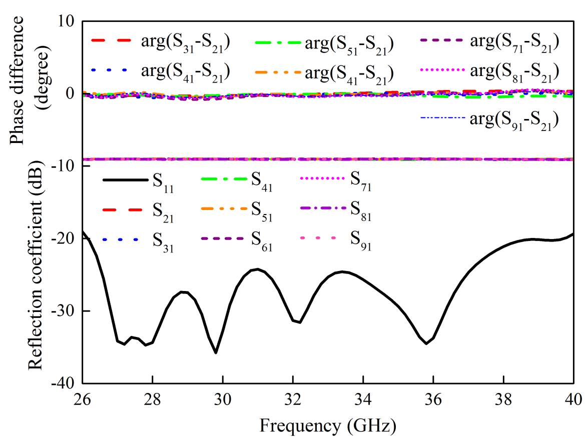

FIGURE 14. Simulated results of the feed network: amplitude and phase responses. The port numbers are shown in Fig. 12.

A. REFLECTION COEFFICIENT

The reflection coefficients are measured using Agilent E8361C network analyzer and shown in Fig. 16. They are in

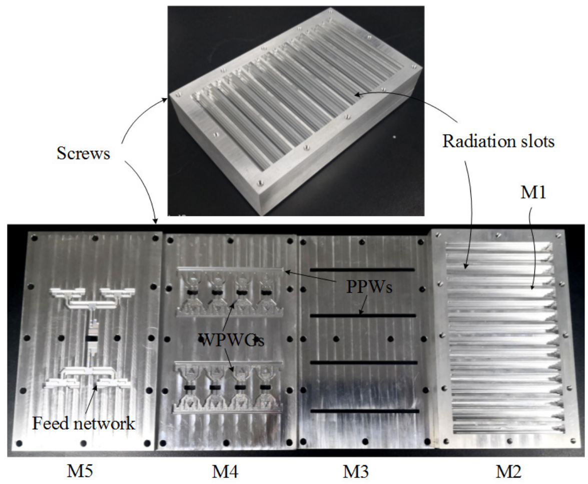

FIGURE 15. Photographs of the fabricated CTS antenna array.

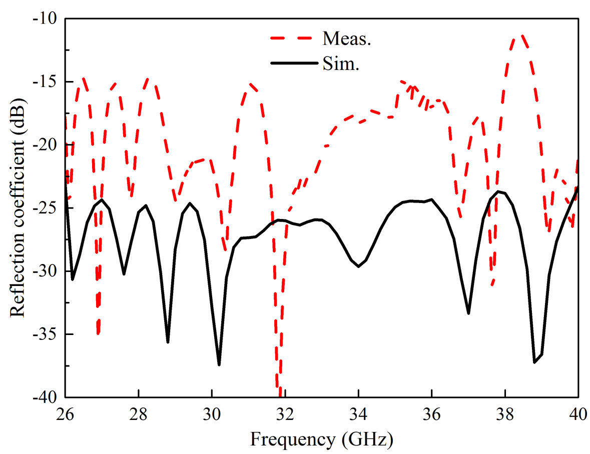

FIGURE 16. Simulated and measured reflection coefficients of the CTS antenna.

reasonably good agreement with simulations. The difference is mainly attributed to the assembly errors and fabrication tolerances. A matching ($|S_{11}| < -10$ dB) bandwidth of 42.4 % is achieved over 26 - 40 GHz.

B. RADIATION PATTERNS

Fig. 17 shows the simulated and measured normalized radiation patterns in the E- and H-planes at different frequencies. The measured results are very consistent with the simulations. The beam-widths at the E- and H-planes are determined by the number of radiations slots and the width of WPWG, respectively. The maximum 3-dB beam-widths are 5.2° and 10.4° at E- and H-planes over the whole band. The sidelobe levels (SLLs) at the E- and H-plane radiation patterns are around −13.3 dB and −12.1 dB. This is consistent with the sidelobes characteristics of an array with a uniform amplitude excitation. The measured cross-polarization levels are also plotted in Fig. 17. It shows a low cross-polarizations of better than −46 dB for both the E- and H-planes.

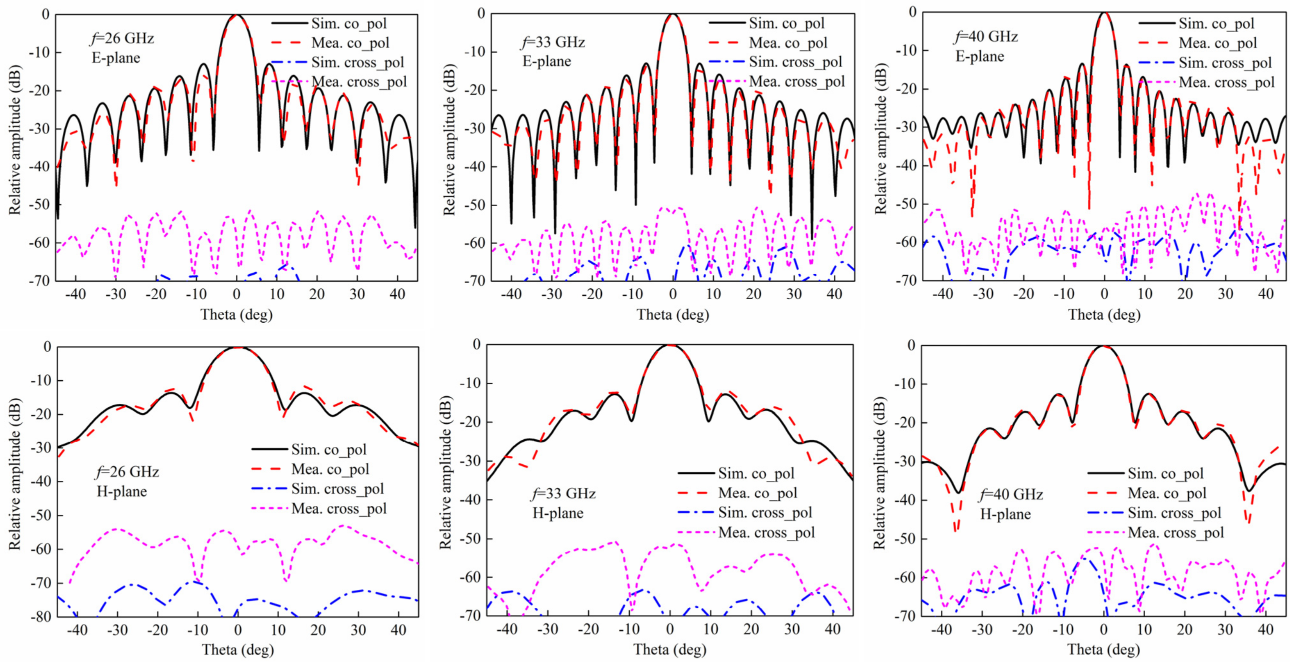

FIGURE 17. Simulated and measured radiation patterns: (a) 26 GHz; (b) 33 GHz; (c) 40 GHz.

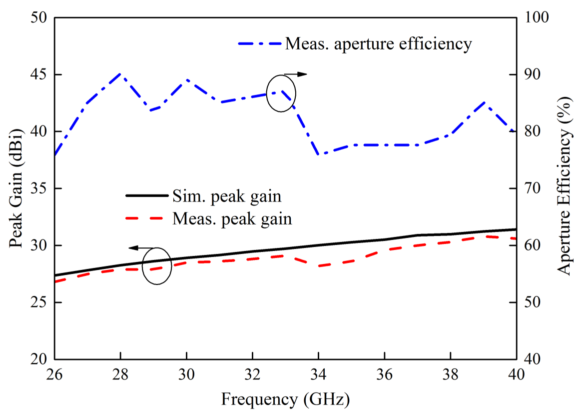

FIGURE 18. Simulated and measured peak gain and aperture efficiency.

C. PEAK GAIN AND APERTURE EFFICIENCY

The measured peak gain and antenna aperture efficiency as a function of the frequency are plotted in Fig. 18. At the center frequency of 33 GHz, a peak gain of 29.1 dBi and an aperture efficiency of 87.1% are recorded. With the help of the wideband WPWG, a high aperture efficiency of more than 75% is achieved over 26 - 40 GHz. The measured peak gain is slightly lower than the simulated. The small difference may be attributed to the assembly error and the fabrication tolerance.

D. COMPARISONS

Table I compares the performance of this design with several other published wideband waveguide arrays. Among them, [15] and [16] are based on SW, others are based on CTS. This work exhibits the largest fractional bandwidth, which is over 42%. Compared with the CTS antenna array in the previous work, the aperture efficiency of this work is improved significantly, due to the high quality quasi-TEM wave generated by the WPWG.

TABLE 1. Comparison of Waveguide Antenna Arrays.

Ref.	Type	Slots No.	BW (%)	Gain (dBi)	Eff. (%)	Size (λ_0^3)*
[15]	SW	16×16	20.4	>31.4	>70	15.7×15.7×0.8
[16]	SW	8×8	30	>25	>80	8.8×8.8×2.4
[19]	CTS	32	19	>30.8	>48	43.2×25.1×8.8
[20]	CTS (LTCC)	4	25.2	>11	>44	6.5×3.4×0.9
This work	CTS	16	42.4	>26.8	>75	12.3×6.7×2.8

* λ_0 is the free space wavelength at the center operating frequency.

IV. CONCLUSION

In this paper, a wideband 16-slot CTS antenna array for Ka-band applications is demonstrated. A WPWG constructed of single-ridge power dividers and PPW is introduced to generate quasi-TEM wave. Compared with the conventional mode converter of pillbox, the proposed WPWG supports a wider operating band and produces quasi-TEM wave with uniform amplitude distribution. To enhance the operating band of the radiation slot, a MSSIT is employed and bandwidth characteristic is examined. For demonstration purpose, an experimental prototype with the operating band was designed and implemented. Experimental results show that the proposed CTS antenna array has an impedance bandwidth of over 42% and aperture efficiency of more than 75% over the whole Ka band. Compared with the previous works, the proposed design shows a wider impedance bandwidth and higher aperture efficiency. It has demonstrated attractive features and potentials for millimeter-wave applications, such as 5G, wideband satellite communication, etc.

REFERENCES

[1] *NR—BS Radio Transmission and Reception*, document TS 38. 104 (V15.2.0), 3GPP, Jun. 2018. [Online]. Available: http://www.3gpp.org/ftp/Specs/archive/38_series/38.104/

[2] A. Vosoogh, M. S. Sorkherizi, A. U. Zaman, J. Yang, and A. A. Kishk, "An integrated Ka-band diplexer-antenna array module based on gap waveguide technology with simple mechanical assembly and no electrical contact requirements," *IEEE Trans. Microw. Theory Techn.*, vol. 66, no. 2, pp. 962–972, Feb. 2018.

[3] W. El-Halwagy, R. Mirzavand, J. Melzer, M. Hossain, and P. Mousavi, "Investigation of wideband substrate-integrated vertically-polarized electric dipole antenna and arrays for mm-wave 5G mobile devices," *IEEE Access*, vol. 6, pp. 2415–2457, 2018.

[4] C. Hannachi and S. O. Tatu, "A compact V-band planar gap-coupled 4×1 antenna array: Improved design and analysis," *IEEE Access*, vol. 5, pp. 8763–8770, 2017.

[5] J. Guo, S. Liao, Q. Xue, and S. Xiao, "Planar aperture antenna with high gain and high aperture efficiency for 60-GHz applications," *IEEE Trans. Antennas Propag.*, vol. 65, no. 12, pp. 6262–6273, Dec. 2017.

[6] Z.-W. Miao *et al.*, "140 GHz high-gain LTCC-integrated transmit-array antenna using a wideband SIW aperture-coupling phase delay structure," *IEEE Trans. Antennas Propag.*, vol. 66, no. 1, pp. 182–190, Jan. 2018.

[7] Z. Chen, H. Liu, J. Yu, and X. Chen, "High gain, broadband and dual-polarized substrate integrated waveguide cavity-backed slot antenna array for 60 GHz band," *IEEE Access.*, vol. 6, pp. 31012–31022, 2018.

[8] Y. She, R. Fujino, J. Hirokawa, M. Ando, D. Hanatani, and M. Fujimoto, "LTCC oversized rectangular waveguide slot array antenna with air-layer in the radiating part in the millimeter-wave band," *IEEE Trans. Antennas Propag.*, vol. 61, no. 4, pp. 1777–1783, Apr. 2013.

[9] Y. Tyagi, P. Mevada, S. Chakrabarty, and R. Jyoti, "High-efficiency broadband slotted waveguide array antenna," *IET Microw., Antennas Propag.*, vol. 11, no. 10, pp. 1401–1408, Aug. 2017.

[10] G.-L. Huang, S.-G. Zhou, T.-H. Chio, H.-T. Hui, and T.-S. Yeo, "A low profile and low sidelobe wideband slot antenna array feb by an amplitude-tapering waveguide feed-network," *IEEE Trans. Antennas Propag.*, vol. 63, no. 1, pp. 419–423, Jan. 2015.

[11] G. P. Le Sage, "3D printed waveguide slot array antennas," *IEEE Access*, vol. 4, pp. 1258–1265, 2016.

[12] Q.-L. Yang, Y.-L. Ban, J.-W. Lian, Z.-F. Yu, and B. Wu, "SIW butler matrix with modified hybrid coupler for slot antenna array," *IEEE Access*, vol. 4, pp. 9561–9569, 2016.

[13] Y. Miura, J. Hirokawa, M. Ando, Y. Shibuya, and G. Yoshida, "Double-layer full-corporate-feed hollow-waveguide slot array antenna in the 60-GHz band," *IEEE Trans. Antennas Propag.*, vol. 59, no. 8, pp. 2844–2851, Aug. 2011.

[14] D. Kim, M. Zhang, J. Hirokawa, and M. Ando, "Design and fabrication of a dual-polarization waveguide slot array antenna with high isolation and high antenna efficiency for the 60 GHz band," *IEEE Trans. Antennas Propag.*, vol. 62, no. 6, pp. 3019–3027, Jun. 2014.

[15] T. Tomura, J. Hirokawa, T. Hirano, and M. Ando, "A 45° linearly polarized hollow-waveguide 16×16-slot array antenna covering 71–86 GHz band," *IEEE Trans. Antennas Propag.*, vol. 62, no. 10, pp. 5061–5067, Oct. 2014.

[16] A. Farahbakhsh, D. Zarifi, and A. U. Zaman, "A mmWave wideband slot array antenna based on ridge gap waveguide with 30% bandwidth," *IEEE Trans. Antennas Propag.*, vol. 66, no. 2, pp. 1008–1013, Feb. 2018.

[17] W. W. Milroy, "The continuous transverse stub (CTS) array: Basic theory experiment and application," in *Proc. Antenna Appl. Symp.*, vol. 2, Sep. 1991, pp. 253–283.

[18] Y. Xu, H. Dong, Y. Liu, and P. Zhang, "Continuous transverse stub (CTS) array antenna," in *Proc. Int. Symp. Antennas Propag. (ISAP)*, Oct. 2012, pp. 1083–1086.

[19] T. Potelon *et al.*, "A low-profile broadband 32-slot continuous transverse stub array for backhaul applications *E*-band," *IEEE Trans. Antennas Propag.*, vol. 65, no. 12, pp. 6307–6316, Dec. 2017.

[20] F. F. Manzillo *et al.*, "A multilayer LTCC solution for integrating 5G access point antenna modules," *IEEE Trans. Microw. Theory Techn.*, vol. 64, no. 7, pp. 2272–2283, Jul. 2016.

[21] F. F. Manzillo, M. Ettorre, M. Casaletti, N. Capet, and R. Sauleau, "Active impedance of infinite parallel-fed continuous transverse stub arrays," *IEEE Trans. Antennas Propag.*, vol. 63, no. 7, pp. 3291–3297, Jul. 2015.

[22] D. M. Pozar, *Microwave Engineering*, 3rd ed. Hoboken, NJ, USA: Wiley, 2012.

[23] F. F. Manzillo, R. Sauleau, N. Capet, and M. Ettorre, "Mode matching analysis of an E-plane 90° bend with a square step in parallel-plate waveguide," *IEEE Antennas Wireless Propag. Lett.*, vol. 16, pp. 2187–2190, 2017.

[24] Y. You, Y. Lu, Q. You, Y. Wang, J. Huang, and M. J. Lancaster, "Millimeter-wave high-gain frequency-scanned antenna based on waveguide continuous transverse stubs," *IEEE Trans. Antennas Propag.*, vol. 66, no. 11, pp. 6370–6375, Nov. 2018.

[25] M. Samardzija, T. Kai, J. Hirokawa, and M. Ando, "Single-layer waveguide feed for uniform plane tem-wave in oversized-rectangular waveguide with hard-surface sidewalls," *IEEE Trans. Antennas Propag.*, vol. 54, no. 10, pp. 2813–2819, Oct. 2006.

[26] Q.-X. Chu, Z.-Y. Kang, Q.-S. Wu, and D.-Y. Mo, "An in-phase output *Ka*-band traveling-wave power divider/combiner using double ridge waveguide couplers," *IEEE Trans. Microw. Theory Techn.*, vol. 61, no. 9, pp. 3247–3253, Sep. 2013.

QINGCHUN YOU received the B.S. degree in mechanical and electronic engineering from Suzhou University, Suzhou, China, in 2015, and the M.S. degree in electronic engineering and computer science from Ningbo University, Ningbo, China, in 2018. His current research interests include microwave and millimeter-wave circuits, slotted waveguides antenna arrays, lens, and beamforming networks.

YUNLONG LU received the B.S. degree in electronic engineering from Ningbo University, Ningbo, China, in 2007, and the M.S. and Ph.D. degrees in electronic engineering from Zhejiang University, Hangzhou, China, in 2010 and 2015, respectively. In 2008, he was a Research Assistant with Nanyang Technological University, Singapore. He is currently a Lecturer with the Faculty of Electrical Engineering and Computer Science, Ningbo University. His research interests include microwave/millimeter-wave circuit integration and devices, antenna arrays, and multiport filtering networks.

YANG YOU received the B.S. degree in communication engineering from Henan Polytechnic University, Jiaozuo, China, in 2015. He is currently pursuing the M.S. degree in electrical engineering with Ningbo University, Ningbo, China. His current research interests include microwave and millimeter-wave circuits and high-gain antenna arrays.

YI WANG (M'09–SM'12) was born in Binzhou, Shandong, China. He received the B.Sc. degree in physics and the M.Sc. degree in condensed matter physics from the University of Science and Technology, Beijing, China, in 1998 and 2001, respectively, and the Ph.D. degree in electronic and electrical engineering from the University of Birmingham, Birmingham, U.K., in 2005. In 2011, he became a Senior Lecturer and, then, a Reader at the University of Greenwich. In 2018, he joined the University of Birmingham as a Senior Lecturer. His current research interests include millimeter-wave and terahertz devices for metrology, communications and sensors, micromachining, microwave circuits based on multiport filtering networks, and filter-antenna integration.

ZHANG-CHENG HAO (M'08–SM'15) received the B.S. degree in microwave engineering from Xidian University, Xi'an, China, in 1997, and the M.S. and Ph.D. degrees in radio engineering from Southeast University, Nanjing, China, in 2002 and 2006, respectively. In 2006, he was a Post-Doctoral Researcher with the Laboratory of Electronics and Systems for Telecommunications, École Nationale Supérieure des Télécommunications de Bretagne, Brittany, France, where he was involved in the development of millimeter-wave antennas. In 2007, he joined the Department of Electrical, Electronic and Computer Engineering, Heriot-Watt University, Edinburgh, U.K., as a Research Associate, where he was involved with developing multilayer integrated circuits and ultra-wide-band components. In 2011, he joined the School of Information Science and Engineering, Southeast University, Nanjing, China, as a Professor. He holds 20 granted patents. He has authored or co-authored over 170 referred journal and conference papers. His current research interests involve microwave and millimeter-wave systems, submillimeter-wave and terahertz components, and passive circuits, including filters, antenna arrays, couplers, and multiplexers.

Dr. Hao has served as a Reviewer for many technique journals, including the IEEE Transactions on Microwave Theory and Techniques, the IEEE Transactions on Antennas and Propagation, the IEEE Antennas and Wireless Propagation Letters, and the IEEE Microwave and Wireless Components Letters and the Guest Editor for the IEEE T-MTT Special Issue on IWS2018. He was a recipient of the Thousands of Young Talents presented by China Government in 2011 and the High Level Innovative and Entrepreneurial Talent presented by Jiangsu, China, in 2012.

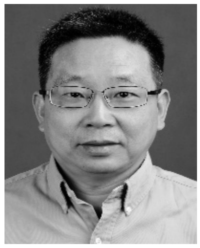

JIFU HUANG received the B.S. and M. S. degrees in radio engineering from Southeast University, China, in 1982 and 1987, respectively, and the Ph.D. degree in electrical and computer engineering from the University of Victoria, Canada, in 1995. From 1982 to 1991, he was a Lecturer with Southeast University. From 1991 to 1994, he was a Research Assistant with the Department of Electrical Engineering, University of Victoria, Canada. From 1994 to 1995, he was a Post-Doctoral Fellow with the Research Center for Advanced Microwave and Space Electronics, Ecole Polytechnique of Montreal, Canada. From 1995 to 2015, he joined the industry at Harris, M/A-COM, Telebeam, 2Wire, and ZTE, Inc., USA, as a Senior to Principal Microwave Engineer. In 2015, he was appointed as a Professor with Ningbo University, China. His research interests include the microwave and millimeter-wave theory, engineering, and applications.